Acta Crystallographica Section B
Structural Science
ISSN 0108-7681

Experimental electron density study of the supramolecular aggregation between 4,4′-dipyridyl-*N*,*N*′-dioxide and 1,4-diiodotetrafluorobenzene at 90 K

Riccardo Bianchi,* Alessandra Forni and Tullio Pilati

CNR, Istituto di Scienze e Tecnologie Molecolari, via Golgi 19, 20133 Milano, Italy

Correspondence e-mail: riccardo.bianchi@istm.cnr.it

Received 12 February 2004
Accepted 14 June 2004

The electron density of the halogen-bonded complex of 4,4′-dipyridyl-*N*,*N*′-dioxide (bpNO) with 1,4-diiodotetrafluorobenzene (F_4dIb) at 90 K has been determined by X-ray diffraction and analysed. The nature of the I···O intermolecular bond connecting the bpNO and F_4dIb molecules into one-dimensional infinite chains, as well as the other non-covalent interactions present in the crystal, such as C—H···O, C—H···F and C—H···I hydrogen bonds and C···C, C···N, C···I and F···F interactions, have been investigated. The integration of electron density over the atomic basins reveals the electrostatic nature of the I···O halogen bond, which is very similar to a previously analysed I···N halogen bond.

1. Introduction

Previous studies have shown that, in addition to hydrogen bonds, crystals contain other relevant intermolecular connections (for example, halogen bonds and stacking interactions) that can assemble molecules into supramolecular architectures (Desiraju & Harlow, 1989; Burling & Goldstein, 1992; Desiraju, 1997; Allen *et al.*, 1998; Choudhury *et al.*, 2002). These molecular interactions appear to be important in crystal engineering and in all fields where aggregation processes have a fundamental role (Desiraju, 1997). In particular, the non-covalent interaction between heavy halogen atoms (I, Br and, to a lesser extent, Cl) and Lewis bases such as nitrogen, oxygen and sulfur has been the subject of several investigations in recent years (Lommerse *et al.*, 1996; Allen *et al.*, 1997; Batsanov *et al.*, 1997; Legon, 1998, 1999*a*,*b*; Nishijo *et al.*, 2000; Metrangolo & Resnati, 2001; Devic *et al.*, 2002; Garden *et al.*, 2002).

Few electron density studies have been carried out for the purpose of fully characterizing the properties of these non-covalent interactions. To this end, we present here an X-ray study at 90 K of the multipole-refined electron density (Stewart, 1976) of the complex of 4,4′-dipyridyl-*N*,*N*′-dioxide (bpNO) with 1,4-diiodotetrafluorobenzene (F_4dIb), in terms of the topological properties of the complex (Bader, 1994*b*). The experimental results will be compared with accurate all-electron theoretical calculations. The bpNO and F_4dIb molecules aggregate into one-dimensional infinite networks, thus giving rise to the shortest I···O intermolecular distance reported to date, and to C—H···O, C—H···F and C—H···I intermolecular hydrogen bonds (Messina *et al.*, 2001). The present work is part of our ongoing project devoted to a systematic electron density study of intermolecular interactions (in particular halogen bonding) in crystals. The topological features of the I···N and C—H···F interactions have been discussed in a previous paper (Bianchi *et al.*, 2003), in which the electron density of the complex of F_4dIb with

Table 1
Experimental details.

Crystal data	
Chemical formula	$C_{10}H_8N_2O_2{\cdot}C_6I_2F_4$
M_r	590.04
Cell setting, space group	Triclinic, $P\overline{1}$
a, b, c (Å)	4.2279 (10), 8.009 (2), 13.569 (3)
α, β, γ (°)	101.180 (5), 98.946 (5), 102.349 (5)
V (Å^3)	430.91 (18)
Z	1
D_x (Mg m^{-3})	2.274
Radiation type	Mo $K\alpha$
No. of reflections for cell parameters	8425
θ range (°)	2.8–59.5
μ (mm^{-1})	3.70
Temperature (K)	90 (2)
Crystal form, colour	Prism, colourless
Crystal size (mm)	0.30 × 0.11 × 0.04
Data collection	
Diffractometer	Bruker SMART APEX CCD area detector
Data collection method	ω and φ scans
Absorption correction	Multi-scan (based on symmetry-related measurements)
T_{min}	0.819
T_{max}	1.000
No. of measured, independent and observed reflections	53 777, 12 612, 12 579
Criterion for observed reflections	$I > 0$
R_{int}	0.027
θ_{max} (°)	60.1
Range of h, k, l	$-8 \Rightarrow h \Rightarrow 9$ $-19 \Rightarrow k \Rightarrow 19$ $-33 \Rightarrow l \Rightarrow 32$
Refinement	
Refinement on	F^2
$R(F^2 > 0)$, $wR(F^2)$, S	0.027, 0.050, 1.01
No. of reflections	12 579
No. of parameters	387
H-atom treatment	Refined independently
Weighting scheme	$w = 1/[\sigma^2(F_o^2)]$
$(\Delta/\sigma)_{max}$	0.001
$\Delta\rho_{max}$, $\Delta\rho_{min}$ (e Å^{-3})	0.22, −0.49

Computer programs used: *SMART* (Bruker, 1997), *SAINT* (Bruker, 1997), *SIR*92 (Altomare *et al.*, 1994), *VALRAY* (Stewart & Spackman, 1983; Stewart *et al.*, 2000), *ORTEP*III (Burnett & Johnson, 1996), *PARST* (Nardelli, 1995).

(*E*)-1,2-bis(4-pyridyl)ethylene (bpe) was analysed. In the present work the topological properties of the I···O and I···N interactions are compared.

Owing to the importance of the electrostatic potential in the study of chemical reactivity and packing interactions, an analysis of this property, as obtained from the diffraction experiment, will be presented.

2. Experimental and computational details

2.1. Data collection and reduction

The synthesis and crystal preparation of the title compound were reported elsewhere (Messina *et al.*, 2001). The crystal used for data collection was glued onto a glass fibre with perfluorinated oil and cooled over a period of 24 h to 90 K by a Kryoflex Bruker N_2 gas stream cooling device. X-ray data were collected on a Bruker SMART APEX CCD area detector and data reduction was performed using *SAINT* (Bruker, 1997); absorption corrections based on multi-scans were obtained using *SADABS* (Bruker, 1997). Experimental details are summarized in Table 1.

Table 2
IAM and multipole refinement information.

	IAM+CUM	POP1+CUM	POP+CUM	POP
Reflections with $\lvert F_o\rvert^2 > 0$	12 579			
No. of parameters	159	401	387	354
$R(F)$	0.0341	0.0323	0.0323	0.0366
$wR(F)$	0.0327	0.0310	0.0310	0.0337
$R(F^2)$	0.0322	0.0273	0.0272	0.0340
$wR(F^2)$	0.0544	0.0504	0.0504	0.0556
S	1.084	1.015	1.014	1.117
k (scale factor)	0.995 (1)	0.976 (3)	0.977 (3)	0.961 (3)
$(\text{shift/s.u.})_{max}$	< 0.01	< 0.01	< 0.01	< 0.01

2.2. Refinements

All refinements were carried out on $\lvert F_o\rvert^2$ using a new version of *VALRAY* (Stewart & Spackman, 1983; Stewart *et al.*, 2000) interfaced by one of us (RB) with the *TOPOND* program (Gatti & Bianchi, 1996; Gatti, 1999). The refinement results are summarized in Table 2. The IAM+CUM model is the conventional refinement of the positional parameters of all atoms, of the anisotropic displacement parameters for I, O, F, N and C atoms, and of the isotropic displacement parameters for H atoms, also including the third- and fourth-order Gram–Charlier terms of the I atom. Atomic and anomalous scattering factors were taken from the *International Tables for Crystallography* (1995, Vol. C).

Recently, Sørensen *et al.* (2003) found, in their charge density study of tetrafluoroterephthalonitrile, that an F atom terminally bonded to an aromatic C atom does not possess significant octopole population parameters. Furthermore, this F atom exhibits a small but significant anharmonic thermal motion that could be modelled by octopole multipole parameters. These results were confirmed from our analysis of several rigid pseudo-atom models (Stewart, 1976) during the refinement process. Initially, the multipole model (POP1+CUM) included the atomic positions and the mean-square amplitudes of vibration of the I, O, F, N and C pseudo-atoms, the third- and fourth-order Gram–Charlier coefficients of the I atom, and only the third-order Gram–Charlier coefficients of the F atoms. H-atom positions were fixed at the values obtained by a previous multipole refinement, with the H atoms polarized in the direction of the atom to which they are bonded, and only the isotropic displacement parameters were refined. For each heavy atom (n), the spherical core electron density and the valence deformation density is a sum of terms expressed by $P_{nlm}R_n(r)Y_{lm}(\theta,\varphi)$, where P_{nlm} is a population parameter, $R_n(r)$ is a radial function of the Slater type or a fixed linear combination of exponentials, and $Y_{lm}(\theta,\varphi)$ is a surface spherical harmonic. At the I-atom position, functional expansions up to hexadecapole level were introduced, whereas the expansions were broken at the octopole level for the F, O, N and C positions, and at the dipole

level for the H atoms. For I, O, F, N and C atoms, the core and valence monopole scattering factors were calculated from Hartree–Fock atomic wavefunctions. A single parameter was refined for the core of all the O, F, N and C atoms. Each H monopole was a single shell, given by $\exp(-2.48r)$. As regards the higher multipoles, the Slater-type exponents (α values) of all the atoms were assigned theory-based fixed values (Hehre *et al.*, 1970).

At the end of the refinement, the octopole population parameters of the F atoms were negligible within the standard uncertainties; we thus decided to omit these parameters in the subsequent refinement (POP+CUM model). Both refinements gave essentially the same results, as reported in Table 2, and very similar residual maps. The crystal electron densities described by the two models showed identical topological features. The inclusion of fourth-order Gram–Charlier coefficients for F atoms in the POP+CUM model did not gave any significant improvement. The final values of these coefficients were largely within the standard uncertainties, unlike the third-order coefficients for the same atoms, which were slightly significant. The residual density was essentially unchanged.

The importance of including anharmonic parameters for I and F atoms in the refinement was also tested by excluding these terms from the POP+CUM model. The final refinement results are reported in Table 2 (POP model); it appears that the POP model can be rejected at the 1% significance level according to the Hamilton (1965) test. The largest residual peaks, 0.9 (2) and −1.1 (2) e Å^{-3}, close to the I atom, were significantly greater than those from the POP+CUM model (see below).

Starting from the POP+CUM model, an additional refinement was carried out in which one α radial exponent for the higher multipoles ($l \geq 1$) of the I atom and κ radial expansion/contraction parameters for C, N and O atoms (one κ for each atomic species) were also varied. All statistical indices, residual maps and topological properties at bond critical points indicated that this multipole model does not lead to a significant improvement with respect to the best POP+CUM model.

The Hirshfeld (1976) rigid-bond test was applied to the final displacement parameters. The r.m.s. of the mean-square displacement amplitudes for bonded atoms along the bond vectors in the title compound was 0.0004 Å; therefore, the final model is consistent with the rigid-bond hypothesis.

Final atomic fractional coordinates, anisotropic and isotropic displacement parameters, third- and fourth-order Gram–Charlier coefficients, multipole populations and electron density maps are provided as supplementary material.[1]

2.3. Theoretical calculations

In order to describe the strongest intermolecular interactions, calculations were performed on a cluster of one molecule of F_4dIb with the four nearest bpNO molecules, using the experimental low-temperature geometry.

Calculations were performed at the RHF and DFT levels using, for the I atom, the split-valence SV2P basis set developed by Andzelm *et al.* (1984) and, for the other atoms, the 6-31G** basis set. The choice of a relatively small basis set for describing the light atoms was dictated by a compromise with the limited basis set available in the literature for iodine. Test calculations on the isolated F_4dIb molecule, including geometry optimization, were also performed using, for I, the SV2PP basis set (Andzelm *et al.*, 1984) instead of SV2P, where a further set of *d* functions is added to this atom, and using the MIDI! basis set (Li *et al.*, 1998) for all atoms. In the latter case the I atom is described with the same degree of accuracy as the other atoms. In all cases, the results of the topological analysis were similar and, in particular, the variations in the net atomic charges were always within 0.1 e.

The wavefunction obtained through these calculations was used for the topological analysis of the electron density. For DFT calculations, the B3LYP functional was used (Lee *et al.*, 1988; Becke, 1993). All the *ab initio* calculations were performed with *Gaussian*98 (Frisch *et al.*, 1998). The *AIMPAC* program (Bader, 1994*a*) was used for the topological analysis of the electron density.

3. Results and discussion

3.1. Structural analysis

The structural details of bpNO·F_4dIb at room temperature (Messina *et al.*, 2001) and in the range 90–292 K (Forni *et al.*, 2004) have been discussed previously. Bond distances, angles and selected intermolecular contacts [nearly within the sum of the van der Waals radii (Bondi, 1964)] from the final multipole refinement (POP+CUM) are reported in Table 3.

The unit cell consists of one bpNO and one F_4dIb molecule, both lying on centres of symmetry. These molecules are connected to each other by I···O halogen bonds, thus forming 1:1 infinite chains in which the two molecules of each bpNO·F_4dIb module are neither perfectly collinear nor

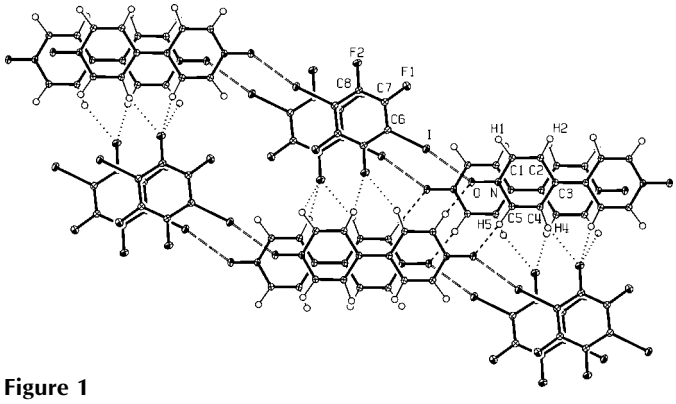

Figure 1
Crystal packing view along the normal to the plane defined by O, N and C5, with the atom-numbering scheme. Long dashed lines: I···O interactions; short dashed lines: C5–H5···O interactions; dotted lines: C—H···F interactions.

[1] Supplementary data for this paper are available from the IUCr electronic archives (Reference: BS5005). Services for accessing these data are described at the back of the journal.

Table 3
Bond lengths (Å), bond angles (°) and selected intermolecular contacts (Å) from the POP+CUM refinement.

An asterisk (*) indicates atomic interactions where a bond path was found.

Intramolecular bond lengths		Intramolecular bond angles		Intermolecular contacts	
C6—I	2.0848 (9)	I—C6—C7	122.06 (7)	I···O	2.7253 (10)*
C6—C7	1.3858 (15)	I—C6—C8^{i}	120.83 (7)	H5···O^{ii}	2.13 (3)*
C6—C8^{i}	1.3903 (15)	C7—C6—C8^{i}	117.05 (8)	H1···F2^{iii}	2.58 (4)*
C7—C8	1.3883 (13)	C6—C7—C8	121.00 (10)	H2···F2^{iv}	2.50 (3)*
C7—F1	1.336 (8)	C6—C7—F1	120.8 (3)	H4···F2^{v}	2.70 (3)*
C8—F2	1.342 (6)	C8—C7—F1	118.2 (4)	H1···I	3.55 (3)
C1—C2	1.3800 (12)	C7—C8—F2	118.1 (3)	H1···I^{vi}	3.56 (4)*
C5—C4	1.3783 (12)	C7—C8—C6^{i}	121.95 (9)	H4···I^{ii}	3.45 (3)*
C2—C3	1.4031 (13)	C6^{i}—C8—F2	119.9 (3)	H5···I^{ii}	3.36 (3)
C4—C3	1.4007 (14)	O—N—C1	120.56 (10)	H5···N^{vii}	2.99 (3)
C3—C3^{viii}	1.4737 (11)	O—N—C5	119.57 (9)	C1···C2^{ix}	3.5613 (15)
C1—N	1.3579 (15)	C1—N—C5	119.87 (9)	C1···O^{vi}	3.4183 (18)
C5—N	1.3582 (13)	N—C1—C2	120.69 (10)	C2···C4^{x}	3.4060 (15)
N—O	1.3010 (12)	C1—C2—C3	121.25 (9)	C3···C3^{x}	3.5512 (18)
C1—H1	1.12 (4)	C2—C3—C4	116.09 (8)	C3···C4^{x}	3.4526 (14)*
C2—H2	1.03 (4)	C2—C3—C3^{viii}	121.87 (11)	C3···C5^{x}	3.5607 (14)
C4—H4	1.08 (3)	C3^{viii}—C3—C4	122.03 (9)	C3···C5^{vi}	3.4194 (14)
C5—H5	1.07 (4)	C3—C4—C5	121.47 (9)	C3···N^{vi}	3.3507 (13)*
		N—C5—C4	120.61 (9)	C4···C5^{vi}	3.5436 (16)
		N—C1—H1	113 (2)	C4···O^{vii}	3.4492 (18)
		C2—C1—H1	126 (2)	C5···C5^{vii}	3.1478 (16)*
		C1—C2—H2	117 (2)	C5···N^{vii}	3.4440 (16)
		C3—C2—H2	121 (2)	C6···C7^{xi}	3.6367 (17)*
		C3—C4—H4	127 (2)	C6···I^{ix}	3.7453 (13)*
		C5—C4—H4	111 (2)	F1···F1^{iii}	3.170 (14)*
		N—C5—H5	115 (2)		
		C4—C5—H5	125 (2)		

Symmetry codes: (i) $-x, -y, -z$; (ii) $2-x, 1-y, 1-z$; (iii) $1-x, 1-y, -z$; (iv) $2-x, 1-y, -z$; (v) $2+x, 1+y, 1+z$; (vi) $1+x, y, z$; (vii) $3-x, 1-y, 1-z$; (viii) $4-x, 2-y, 1-z$; (ix) $x-1, y, z$; (x) $3-x, 2-y, 1-z$; (xi) $1-x, -y, -z$.

coplanar (see Fig. 1). Parallel halogen-bonded chains are linked by a short H5···O($2-x, 1-y, 1-z$) contact and by H2···F2($2-x$, $1-y$, $-z$), H4···F2($2+x$, $1+y$, $1+z$) and H4···I($2-x$, $1-y$, $1-z$) hydrogen bonds (Thalladi *et al.*, 1998) [C—H···X = 168 (3), 146 (2), 148 (2) and 132 (2)°, respectively], thus forming corrugated molecular planes. These planes are connected to each other by H1···F2($1-x$, $1-y$, $-z$) and H1···I($1+x, y, z$) hydrogen bonds [C—H···X 108 (2) and 100 (2)°, respectively] and by π–π interactions involving, separately, dipyridyl and diiodofluorobenzene molecules. Moreover, dipyridyl molecules stacked along the [100] direction are shifted laterally with respect to each other so as to allow a dipole–quadrupole interaction between the N—O bond of one molecule and the pyridyl ring of the other.

3.2. Difference density maps

The residual density maps, obtained by a Fourier synthesis for which the coefficients are the differences $F_{\rm observed} - F_{\rm multipole}$, are illustrated in Fig. 2. The largest peak, 0.22 (9) e Å^{-3}, is close to the I nucleus. The estimated standard uncertainty (σ) of the residual density in the bonding regions is 0.1 e Å^{-3}. All the features in the residual map are $\leq 3\sigma$ [except for the negative hole of −0.49 (9) e Å^{-3} near the I nucleus], indicating that the POP+CUM model used in the refinement is adequate. As described in §2.2, this model does not include the octopole parameters for the F atoms because they are not significant. These atoms, however, possess an appreciable anharmonic motion, as discussed by Sørensen *et al.* (2003).

The deformation density maps, calculated with Fourier coefficients $F_{\rm observed} - F_{\rm IAM}$, are reported in Fig. 3.

Bonding density is observed in every C—I, C—F, N—O, C—C, C—N and C—H bond. Lone-pair density accumulation is evident around the F and O atoms. The presence of the I···O and C5—H5···O intermolecular bonds implies that the O atoms are clearly polarized towards the I and H5 atoms.

3.3. Topological analysis

The electron density, $\rho(\mathbf{r})$, and its Laplacian, $\nabla^2\rho(\mathbf{r})$, were analysed using the quantum theory of atoms in molecules (QTAIM; Bader, 1994*b*). A bond critical point (BCP) is a saddle point where $\nabla\rho(\mathbf{r}) = 0$. The curvatures λ_1, λ_2 and λ_3 ($\lambda_1 < 0$, $\lambda_2 < 0$ and $\lambda_3 > 0$) are the three non-zero eigenvalues of the Hessian matrix of $\rho(\mathbf{r})$ at the BCP.

For the title complex, the properties of the experimental and theoretical electron density at the BCPs are reported in Tables 4 and 5. Fig. 4 shows the experimental Laplacian, $\nabla^2\rho(\mathbf{r})$.

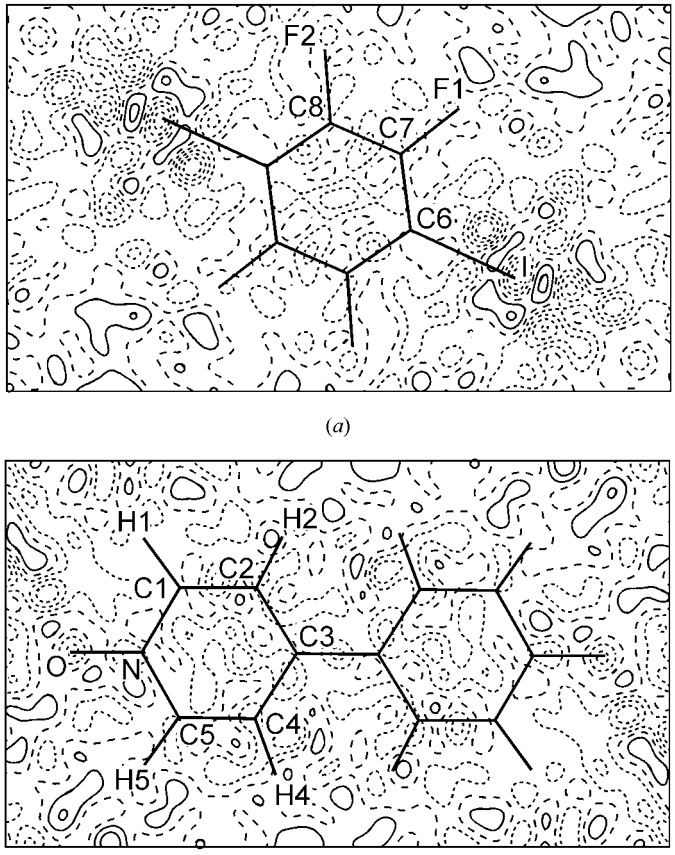

Figure 2
Residual density maps in the least-squares plane defined by the heavy atoms of (*a*) the F_4dIb and (*b*) the bpNO molecules. The contour interval is 0.10 e Å^{-3}. Solid lines: positive contours; short dashed lines: negative contours; wide dashed lines: zero contours.

The Laplacian map in Fig. 4 shows a shell structure in the valence region of the electron density of each atom. In particular, the N and C atoms in both the bpNO and the F_4dIb molecules have the expected sp^2-hybridization of the *L*-shell structure.

The depletion of the electron density at the centre of the two molecular rings is practically the same (see the bottom of Table 4). A similar trend is observed for the depletion of the intermolecular rings reported at the bottom of Table 5; this depletion is lower by a mean factor of approximately six; two of these regions are clearly visible in Fig. 4.

The topological properties of the F_4dIb molecule are in very close agreement with the corresponding properties found in the bpe·F_4dIb complex (Bianchi *et al.*, 2003); therefore, only the main features will be summarized below. The C6—I bond is characterized at the BCP by a relatively low electron density, ρ_{BCP}, of 0.73 (2) e Å^{-3} and a positive Laplacian, $\nabla^2\rho_{BCP}$, of 2.1 (2) e Å^{-5}. The λ_1 and λ_2 curvatures are much smaller than the bond parallel curvature (λ_3), in agreement with a flat $\rho(\mathbf{r})$ on the interatomic surface. The topological values of the C—C and C—F bonds are typical of the covalent and polar covalent interactions, respectively (see Table 4). The experimentally derived topological properties at the BCPs are generally well reproduced by the theoretical calculations, with the exception of the highly polar C—F bonds, for which experiment and theory give very different λ_3 values. These discrepancies can be ascribed to both the nature of the radial functions used in the multipolar model and the inadequacy of the basis set used in the theoretical calculations (Koritsanszky & Coppens, 2001).

As for the bpNO molecule, all the bonds are characterized by high values of ρ_{BCP} (mean 2.09 e Å^{-3}) and large negative values of $\nabla^2\rho_{BCP}$ (mean −17.7 e Å^{-5}), in agreement with those of typical covalent bonds. The only exception is observed for the polar N—O bond, for which $\nabla^2\rho_{BCP} = 0$. However, this anomalous value is determined by the very large curvature λ_3, which is overestimated by the multipole model (see Table 4) in a manner similar to that observed by Bianchi *et al.* (1996).

Chemical bonds can also be characterized by the local electronic energy density (Bader & Beddall, 1972), $H_{BCP} = G_{BCP} + V_{BCP}$, where G_{BCP} and V_{BCP} indicate, respectively, the values of the kinetic and potential energy densities at the BCP, and can be estimated within the Abramov approximation

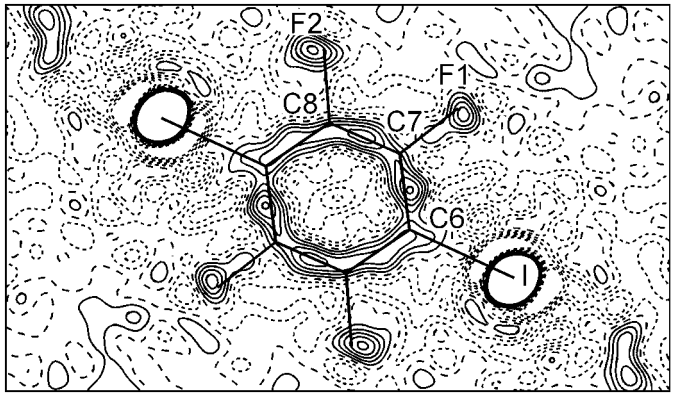

(*a*)

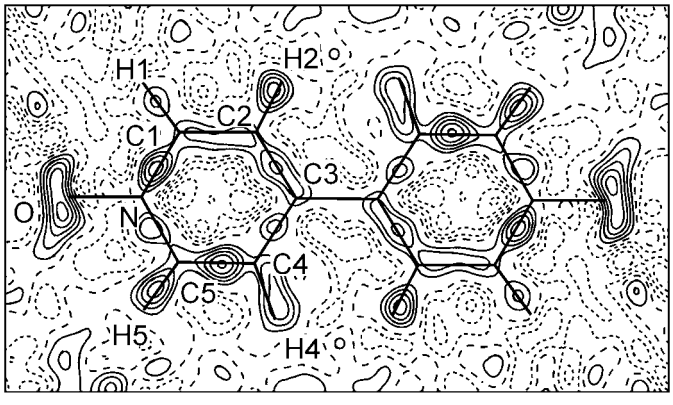

(*b*)

Figure 3
Deformation density maps, as in Fig. 2.

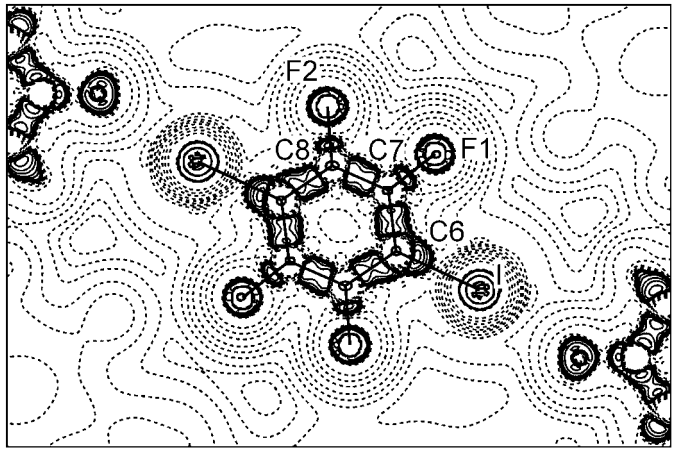

(*a*)

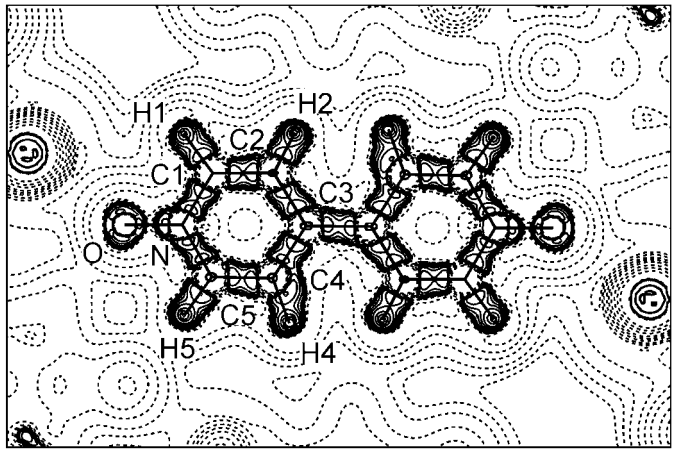

(*b*)

Figure 4
Laplacian, $\nabla^2\rho(\mathbf{r})$, of the experimental electron density map in the same planes as Fig. 2. The absolute values of the contours (e Å^{-5}) increase from the outermost inwards in steps of 0.5×10^n, 1×10^n, 2×10^n, with n beginning at −1 and increasing in steps of 1. Positive values are denoted by dashed contours; negative values are denoted by solid contours.

Table 4
Bond critical-point properties from the POP+CUM model.

R_x = distance between atom X and the BCP; R_e = distance between atoms X and Y. First row: experimental POP+CUM model; second and third rows: theoretical DFT and RHF calculations.

$X-Y$	R_x (Å)	R_x/R_e	ρ_{BCP} (e Å^{-3})	$\nabla^2\rho_{BCP}$ (e Å^{-5})	λ_1 (e Å^{-5})	λ_2 (e Å^{-5})	λ_3 (e Å^{-5})
Intramolecular bond critical points							
C6—I	1.018	0.49	0.73 (2)	2.1 (2)	−2.79	−2.18	7.03
	1.043	*0.50*	*0.82*	*2.3*	*−2.87*	*−2.74*	*7.95*
	1.068	*0.51*	*0.82*	*3.9*	*−2.85*	*−2.73*	*9.53*
C6—C7	0.604	0.44	2.14 (7)	−23 (3)	−19.30	−13.94	10.06
	0.673	*0.49*	*2.16*	*−21.7*	*−16.42*	*−12.78*	*7.50*
	0.664	*0.48*	*2.23*	*−24.8*	*−17.63*	*−13.49*	*6.27*
C6—C8^{i}	0.667	0.48	2.12 (6)	−20 (2)	−19.29	−13.83	12.93
	0.674	*0.48*	*2.14*	*−21.2*	*−16.20*	*−12.59*	*7.55*
	0.665	*0.48*	*2.21*	*−24.3*	*−17.38*	*−13.29*	*6.32*
C7—C8	0.711	0.51	2.30 (6)	−26 (2)	−22.87	−15.45	11.90
	0.693	*0.50*	*2.19*	*−22.6*	*−17.66*	*−12.74*	*7.79*
	0.692	*0.50*	*2.26*	*−25.9*	*−19.08*	*−13.45*	*6.67*
C7—F1	0.546	0.41	2.14 (9)	−25 (4)	−22.74	−17.53	15.59
	0.440	*0.33*	*1.77*	*5.2*	*−12.03*	*−11.93*	*29.16*
	0.426	*0.32*	*1.74*	*11.2*	*−13.32*	*−12.59*	*37.12*
C8—F2	0.518	0.39	1.91 (9)	−22 (4)	−19.36	−15.02	12.40
	0.442	*0.33*	*1.73*	*5.1*	*−11.44*	*−11.32*	*27.82*
	0.427	*0.32*	*1.70*	*11.4*	*−12.57*	*−11.90*	*35.85*
C1—C2	0.689	0.50	2.13 (6)	−21 (2)	−18.71	−13.59	11.66
	0.711	*0.52*	*2.17*	*−21.9*	*−16.30*	*−12.91*	*7.35*
	0.722	*0.52*	*2.23*	*−25.1*	*−17.48*	*−13.72*	*6.08*
C5—C4	0.668	0.48	2.20 (6)	−19 (2)	−19.48	−13.31	13.58
	0.705	*0.51*	*2.19*	*−22.2*	*−16.49*	*−13.19*	*7.46*
	0.713	*0.52*	*2.25*	*−25.6*	*−17.72*	*−14.12*	*6.24*
C2—C3	0.695	0.50	2.10 (6)	−19 (2)	−18.36	−13.40	12.75
	0.703	*0.50*	*2.08*	*−20.2*	*−15.26*	*−12.85*	*7.95*
	0.695	*0.50*	*2.14*	*−23.0*	*−16.34*	*−13.45*	*6.82*
C4—C3	0.641	0.46	1.99 (6)	−17 (2)	−16.16	−12.56	11.27
	0.703	*0.50*	*2.09*	*−20.4*	*−15.31*	*−12.94*	*7.90*
	0.696	*0.50*	*2.15*	*−23.1*	*−16.39*	*−13.50*	*6.77*
C3—C3^{ii}	0.737	0.50	1.69	−13	−13.99	−10.53	11.44
	0.739	*0.50*	*1.83*	*−16.3*	*−12.99*	*−11.75*	*8.48*
	0.740	*0.50*	*1.90*	*−19.5*	*−14.03*	*−12.98*	*7.46*
C1—N	0.563	0.41	2.39 (8)	−29 (3)	−22.73	−18.81	12.80
	0.450	*0.33*	*2.16*	*−13.4*	*−16.25*	*−13.86*	*16.69*
	0.433	*0.32*	*2.18*	*−8.9*	*−17.58*	*−15.34*	*23.98*
C5—N	0.557	0.41	2.23 (8)	−24 (3)	−20.13	−15.35	11.93
	0.447	*0.33*	*2.14*	*−11.5*	*−15.49*	*−14.11*	*18.09*
	0.431	*0.32*	*2.15*	*−6.7*	*−16.67*	*−15.65*	*25.66*
N—O	0.648	0.50	2.67 (7)	0 (2)	−24.45	−21.46	45.95
	0.637	*0.49*	*2.75*	*−14.5*	*−23.00*	*−21.31*	*29.83*
	0.657	*0.50*	*2.79*	*−17.0*	*−23.06*	*−21.62*	*27.72*
C1—H1	0.791	0.71	1.59 (8)	−15 (3)	−17.50	−16.25	18.46
	0.720	*0.64*	*1.82*	*−22.9*	*−17.59*	*−16.92*	*11.62*
	0.720	*0.64*	*1.88*	*−25.4*	*−18.30*	*−17.68*	*10.58*
C2—H2	0.664	0.64	2.01 (9)	−21 (3)	−21.15	−18.49	18.79
	0.643	*0.62*	*2.16*	*−31.6*	*−21.27*	*−20.98*	*10.68*
	0.633	*0.61*	*2.20*	*−33.8*	*−21.68*	*−21.28*	*9.18*
C4—H4	0.722	0.67	1.96 (10)	−17 (2)	−20.58	−19.15	22.44
	0.683	*0.63*	*1.93*	*−25.0*	*−18.33*	*−18.09*	*11.43*
	0.677	*0.63*	*1.97*	*−27.1*	*−18.79*	*−18.44*	*10.17*
C5—H5	0.747	0.70	1.91 (10)	−18 (3)	−21.01	−19.51	22.54
	0.708	*0.66*	*2.05*	*−30.5*	*−21.22*	*−20.55*	*11.28*
	0.715	*0.67*	*2.11*	*−33.9*	*−22.27*	*−21.67*	*10.04*
Ring critical points							
C6—C7—C8—C6^{i}—C7^{i}—C8^{i}			0.14 (1)	2.37 (9)	−0.09	0.92	1.54
			0.13	*3.74*	*−0.34*	*1.99*	*2.08*
			0.13	*3.70*	*−0.28*	*1.95*	*2.03*
N—C1—C2—C3—C4—C5			0.20 (1)	2.87 (7)	−0.32	1.49	1.70
			0.14	*4.05*	*−0.40*	*1.85*	*2.59*
			0.14	*4.07*	*−0.36*	*1.86*	*2.56*

See Table 1 for symmetry codes.

(Abramov, 1997; Espinosa *et al.*, 1998). Recently, Espinosa *et al.* (2002) proposed a classification scheme for atomic interactions, which divides them into three characteristic regions: *pure* closed shell (region I, $\nabla^2\rho_{BCP} > 0$, $H_{BCP} > 0$), *transit* closed shell (region II, $\nabla^2\rho_{BCP} > 0$, $H_{BCP} < 0$) and *pure* shared shell (region III, $\nabla^2\rho_{BCP} < 0$, $H_{BCP} < 0$). The boundaries between regions I, II and III are defined by $H_{BCP} = 0$ (*i.e.* $|V_{BCP}|/G_{BCP} = 1$) and by $\nabla^2\rho_{BCP} = 0$ (*i.e.* $|V_{BCP}|/G_{BCP} = 2$). Inside region I, the bond-degree parameter (BD = H_{BCP}/ρ_{BCP}) is an index of non-covalent interaction and indicates the softening degree (SD) per electron density unit at the BCP; the weaker the interaction, the greater the SD magnitude. In regions II and III, the BD parameter measures the covalence degree (CD) of any pairwise interaction; the stronger the interaction, the greater the CD magnitude. It should be noted that the Abramov approximation largely overestimates both G_{BCP} and V_{BCP} magnitudes for covalent bonds. However, these errors are largely compensated in calculating H_{BCP} and the ratio $|V_{BCP}|/G_{BCP}$, which are then qualitatively comparable to the corresponding 'exact' theoretical values, as shown below.

For the C6—I bond, the experimental ratio $|V_{BCP}|/G_{BCP}$ is 1.7 (*c.f.* the theoretical values 1.71 and 1.58 obtained at the DFT and RHF levels), so this bond can be described as a *transit* closed-shell interaction. For the remaining bonds, the mean value is 2.8 (4.8/5.6 at the DFT/RHF levels), so these bonds are considered as *pure* shared-shell type. Therefore, the ratio $|V_{BCP}|/G_{BCP}$ indicates a partially covalent character for the C6—I bond and a covalent nature for the other bonds of the bpNO·F_4dIb complex. The covalence degree parameter indicates that the C6—I bond (CD = −0.58) is weaker than the N—O, C—C, C—N and C—H bonds, which have a significantly larger CD magnitude (−1.54 on average). The corresponding theoretical DFT/RHF CD values are −0.48/−0.47 for the C6—I bond and −1.15/−1.18, on average, for all the other bonds.

In Table 5, the intermolecular interactions for which a bond path was found are listed. The magnitudes of the topological properties at the I···O BCP indicate that this interaction is comparable to an O—H···O hydrogen bond of medium strength (Espinosa *et al.*, 1999) and to the I···N halogen bond (Bianchi *et al.*, 2003). Using the formula tested by Espinosa *et al.* (1998) for the calculation of the hydrogen-bond energy, $E_{HB} = 0.5V_{BCP}$, the strength of the I···O bond is 31 kJ mol^{-1}. The estimated energy of this interaction is close to that obtained for the I···N bond (36 kJ mol^{-1}; Bianchi *et al.*, 2003) and more than twice the estimated E_{HB} value for the C5—H5···O hydrogen bond (13 kJ mol^{-1}); the latter estimate lies in the range of theoretical and experimental values reported in the literature (Desiraju & Steiner, 1999). Within the limits of such a simple formula, these results give an indication of the relative strength of the interactions studied. The estimated E_{HB} energy for the I···O bond is well reproduced by DFT calculations for the bpNO·F_4dIb dimer at the fully optimized geometry, using the *Gaussian*98 SDD keyword [Dunning/Huzinaga valence double-zeta on C, N, O, F and H, and Stuttgart/Dresden effective core potential (Leininger *et al.*,

Table 5
Experimental (POP+CUM model) bond critical-point properties of intermolecular interactions for which a bond path was found.

Theoretical DFT and RHF results, when available, are given in the second and third rows, respectively.

$X\cdots Y$	R_x (Å)	R_x/R_e	ρ_{BCP} (e Å^{-3})	$\nabla^2\rho_{BCP}$ (e Å^{-5})	λ_1 (e Å^{-5})	λ_2 (e Å^{-5})	λ_3 (e Å^{-5})	G_{BCP} (H Å^{-3})	V_{BCP} (H Å^{-3})	H_{BCP} (H Å^{-3})	$\lvert V_{BCP}\rvert/G_{BCP}$	H_{BCP}/ρ_{BCP}
Halogen bond												
I···O	1.512	0.55	0.201 (4)	2.04 (6)	−0.61	−0.57	3.22	0.151 (3)	−0.158 (8)	−0.008 (9)	1.05 (6)	−0.04 (4)
	1.484	*0.54*	*0.170*	*1.94*	*−0.45*	*−0.42*	*2.82*	*0.131*	*−0.126*	*0.005*	*0.97*	*0.03*
	1.461	*0.54*	*0.156*	*1.96*	*−0.38*	*−0.34*	*2.69*	*0.133*	*−0.129*	*0.004*	*0.97*	*0.03*
Hydrogen bonds												
H5···O^{iv}	0.826	0.39	0.090 (17)	1.74 (8)	−0.39	−0.37	2.50	0.096 (6)	−0.070 (13)	0.026 (15)	0.73 (14)	0.29 (18)
	0.814	*0.38*	*0.125*	*1.25*	*−0.53*	*−0.50*	*2.27*	*0.091*	*−0.094*	*−0.003*	*1.04*	*−0.02*
	0.796	*0.37*	*0.118*	*1.31*	*−0.50*	*−0.46*	*2.27*	*0.095*	*−0.098*	*−0.003*	*1.03*	*−0.03*
H1···F2^{vi}	1.258	0.49	0.042 (3)	0.69 (2)	−0.13	−0.11	0.93	0.036 (1)	−0.024 (3)	0.012 (3)	0.67 (9)	0.29 (7)
H2···F2^{vii}	1.083	0.43	0.032 (7)	0.67 (3)	−0.12	−0.11	0.89	0.034 (2)	−0.021 (4)	0.013 (4)	0.62 (12)	0.41 (15)
	1.047	*0.42*	*0.047*	*0.72*	*−0.18*	*−0.17*	*1.08*	*0.042*	*−0.034*	*0.008*	*0.81*	*0.17*
	1.043	*0.42*	*0.044*	*0.76*	*−0.18*	*−0.17*	*1.10*	*0.045*	*−0.036*	*0.009*	*0.80*	*0.20*
H4···F2^{viii}	1.181	0.44	0.019 (5)	0.41 (3)	−0.06	−0.04	0.50	0.020 (2)	−0.012 (4)	0.008 (4)	0.58 (21)	0.45 (24)
	1.159	*0.43*	*0.029*	*0.49*	*−0.10*	*−0.07*	*0.67*	*0.026*	*−0.018*	*0.008*	*0.69*	*0.28*
	1.153	*0.43*	*0.026*	*0.51*	*−0.10*	*−0.07*	*0.68*	*0.027*	*−0.019*	*0.008*	*0.69*	*0.31*
H1···I^{x}	1.544	0.43	0.029 (1)	0.28 (1)	−0.05	−0.03	0.37	0.015 (1)	−0.011 (1)	0.004 (1)	0.72 (8)	0.15 (3)
H4···I^{iv}	1.338	0.39	0.023 (2)	0.26 (2)	−0.04	−0.02	0.32	0.014 (1)	−0.009 (2)	0.005 (3)	0.67 (15)	0.20 (13)
	1.228	*0.36*	*0.028*	*0.27*	*−0.06*	*−0.06*	*0.39*	*0.015*	*−0.011*	*0.004*	*0.72*	*0.14*
	1.216	*0.35*	*0.027*	*0.29*	*−0.06*	*−0.06*	*0.41*	*0.016*	*−0.011*	*0.005*	*0.72*	*0.19*
Other intermolecular interactions												
C3···C4^{ix}	1.889	0.55	0.044 (1)	0.47 (1)	−0.04	−0.03	0.54	0.026 (1)	−0.020 (1)	0.007 (1)	0.75 (5)	0.15 (2)
C3···N^{x}	1.674	0.50	0.041 (1)	0.48 (1)	−0.07	−0.01	0.55	0.026 (1)	−0.020 (1)	0.007 (1)	0.72 (5)	0.18 (2)
C5···C5^{v}	1.574	0.50	0.060 (2)	0.67 (2)	−0.12	−0.05	0.84	0.039 (1)	−0.030 (3)	0.008 (3)	0.79 (8)	0.14 (5)
C6···C7^{xi}	1.825	0.50	0.029 (1)	0.32 (1)	−0.04	0.00	0.36	0.017 (1)	−0.012 (1)	0.005 (1)	0.69 (7)	0.18 (4)
C6···I^{iii}	2.032	0.54	0.044 (1)	0.42 (1)	−0.07	−0.02	0.52	0.024 (1)	−0.019 (1)	0.005 (1)	0.78 (5)	0.12 (2)
F1···F1^{vi}	1.585	0.50	0.016 (1)	0.323 (4)	−0.05	−0.04	0.42	0.016 (1)	−0.009 (1)	0.007 (1)	0.58 (7)	0.42 (7)
Intermolecular ring critical points												
C2—C3—C4···C2^{ix}—C3^{ix}—C4^{ix}			0.041 (1)	0.45 (1)	−0.05	0.02	0.48					
C6—C7···C6^{xi}—C7^{xi}			0.029 (1)	0.32 (1)	−0.04	0.00	0.36					
I···H4 ^{iv}—C4^{iv}—C5^{iv}—H5^{iv}···O			0.023 (2)	0.25 (1)	−0.04	0.02	0.27					
			0.022	*0.25*	*−0.04*	*0.07*	*0.22*					
			0.021	*0.27*	*−0.04*	*0.07*	*0.23*					
O—N—C5—H5···O ^{iv}—N^{iv}—C5^{iv}—H5^{iv}			0.022 (2)	0.35 (1)	−0.05	0.14	0.26					
			0.027	*0.40*	*−0.08*	*0.16*	*0.32*					
			0.023	*0.42*	*−0.07*	*0.16*	*0.33*					

See Table 1 for symmetry codes.

1996, and references therein) on I]. The computed energies, uncorrected and corrected for basis set superposition error (Boys & Bernardi, 1970), are 33 and 26 kJ mol^{-1}, respectively.

Generally, the multipole model reproduces the effects of the intermolecular interactions in agreement, within 2σ, with the theoretical calculations. The BCP properties reveal a *pure* closed-shell character (see Table 5); in fact, the ratio $|V_{BCP}|/G_{BCP}$ is always less than 1, except for the experimental and theoretical values of the I···O and H5···O bonds, respectively. However, these interactions can also be associated with *pure* closed-shell-type interactions (region I) within the experimental uncertainties and the limits of the theoretical models.

The C5—H5···O, C—H··· and C—H···I hydrogen bonds have experimental ρ_{BCP} and $\nabla^2\rho_{BCP}$ values within the ranges 0.019–0.090 e Å^{-3} and 0.26–1.74 e Å^{-5}, respectively. The values of the corresponding softening degree parameters (SD = H_{BCP}/ρ_{BCP}) are indicative of their relative strength; the two strongest interactions involve the I atom.

To further characterize the interactions between bpNO and F_4dIb molecules in the crystal, the topology of the Laplacian, $\nabla^2\rho(\mathbf{r})$, has been analysed. The critical points of $\nabla^2\rho(\mathbf{r})$ can be classified by the pair (ω,σ), where ω is the number of non-zero eigenvalues of the Hessian matrix associated with $\nabla^2\rho(\mathbf{r})$ and σ is the number of positive eigenvalues minus the number of negative values. The experimental distribution of $\nabla^2\rho(\mathbf{r})$ shows two (3,+3) critical points in the valence shell charge concentration (VSCC) associated with the O atom, one pointing towards the I atom (ρ_{BCP} = 6.34 e Å^{-3}, $\nabla^2\rho_{BCP}$ = −138.5 e Å^{-5}) and the other towards atom H5($2-x$, $1-y$, $1-z$) (ρ_{BCP} = 6.58 e Å^{-3}, $\nabla^2\rho_{BCP}$ = −155.1 e Å^{-5}). One (3,−3) critical point in the VSCC associated with atom C6 is positioned in the direction of the I atom (ρ_{BCP} = 1.76 e Å^{-3}, $\nabla^2\rho_{BCP}$ = −27.9 e Å^{-5}). Four (3,+3) critical points were found in the valence shell charge-depletion region associated with the I atom (distance from I = 1.16 Å, ρ_{BCP} = 0.36 e Å^{-3}, $\nabla^2\rho_{BCP}$ = +0.5 e Å^{-5} on average); these points are located far from the directions of the intra- and intermolecular interactions.

Table 6
Integrated net charge q (e) of the atomic basins Ω by the QTAIM partitioning.

Ω	Experimental	DFT	RHF
I	−0.26	0.35	0.43
F1	−0.60	−0.64	−0.74
F2	−0.64	−0.65	−0.75
C6	0.14	−0.24	−0.25
C7	0.51	0.59	0.67
C8	0.65	0.57	0.63
O	−0.44	−0.63	−0.73
N	−0.54	−0.71	−0.92
C1	0.34	0.47	0.59
C2	−0.03	0.07	0.13
C3	−0.03	0.03	0.03
C4	−0.09	0.02	0.06
C5	0.25	0.47	0.58
H1	0.42	0.09	0.09
H2	0.05	0.00	−0.04
H4	0.06	0.03	0.01
H5	0.21	0.16	0.19

A close examination of the shortest contacts in the crystal [*i.e.* with interatomic separations approximately within the van der Waals contact distance (Bondi, 1964)] showed the presence of other important intermolecular interactions, as revealed by the existence of a bond path connecting the interacting atoms. The BCP properties of these interactions are reported in Table 5. The C3$\cdots$C4$(3-x, 2-y, 1-z)$ and C5$\cdots$C5$(3-x,\ 1-y,\ 1-z)$ distances between stacked bpNO molecules, and the C6$\cdots$C7$(1-x, -y, -z)$ distance between stacked F_4dIb molecules, are indicative of π–π interactions between aromatic rings. The bond paths are characterized by a strong curvature near the nuclear attractors. Similar behaviour is observed for the I$\cdots$C6$(1+x, y, z)$ interaction (near the C6 nucleus) between the I atom and the π system of the benzene ring. The C3$\cdots$N$(1+x, y, z)$ interaction between the π system of bpNO and the NO dipole shows a different shape of bond path, with less pronounced curvature near the nuclear attractors. The strength associated with all these interactions is comparable to that of the C—H$\cdots$I hydrogen bonds, as revealed by the corresponding SD = H_{BCP}/ρ_{BCP} values.

Another short interatomic distance was found between atoms F1 and F1$(1-x,\ 1-y,\ -z)$; this contact connects adjacent F_4dIb molecules in the same plane. The presence of such weak F$\cdots$F interactions can be interpreted as the consequence of a favourable energetic balance between these interactions and the other intermolecular interactions in the plane (for example, I$\cdots$O halogen bonds and C—H$\cdots$F hydrogen bonds).

In Table 6 the atomic charges, calculated from integration over the topological atomic basins Ω, are reported (Bader, 1994*b*). In the F_4dIb molecule ($q \simeq -0.4$ e) the I atom has a negative charge of −0.26 e, the F atoms are negative ($q \simeq -0.6$ e) and the C atoms have a positive net charge. In the bpNO molecule ($q \simeq 0.4$ e) the NO group is highly negative, atoms C2, C3 and C4 are essentially neutral, while the positive net charge is concentrated around atoms C1 and C5, and the H atoms. The charge transfer of nearly 0.4 e between the bpNO and F_4dIb molecules is of the same magnitude as that found in the bpe·F_4dIb complex.

The comparison between experimental and theoretical net atomic charges shows a roughly similar trend, the better

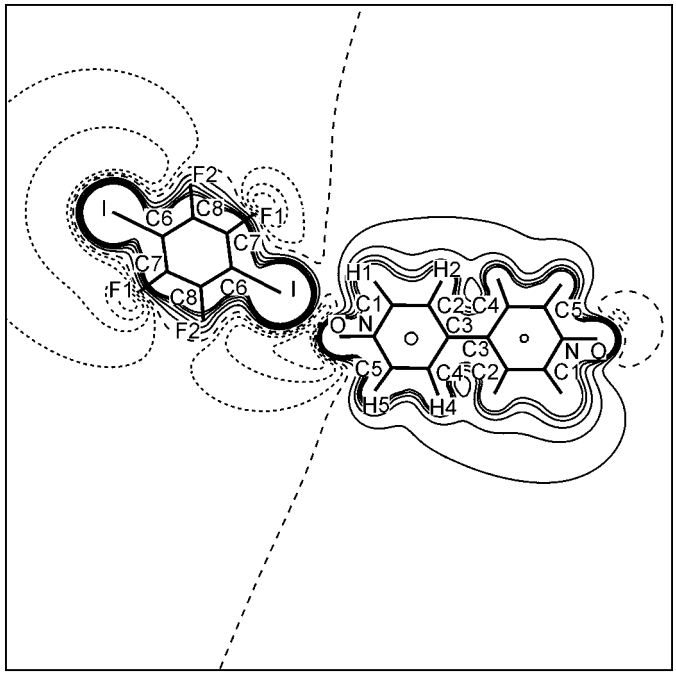

(*a*)

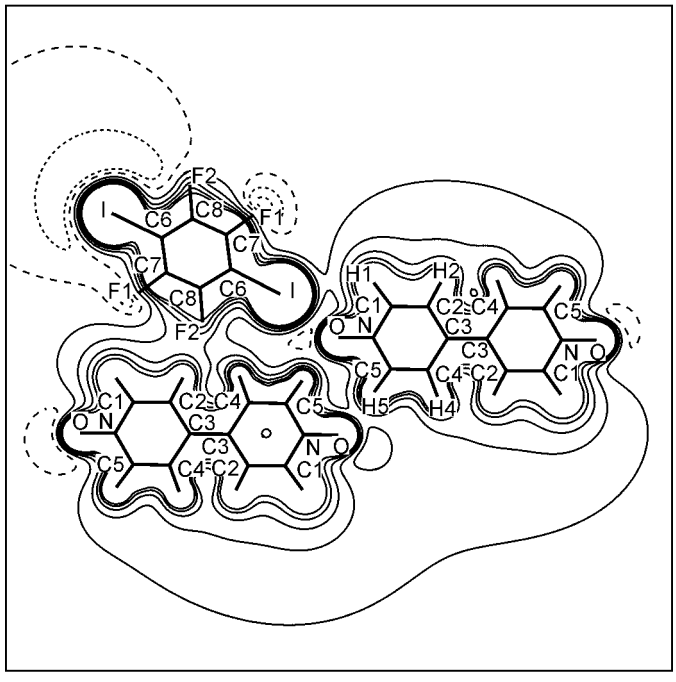

(*b*)

Figure 5
Electrostatic potential for (*a*) bpNO·F_4dIb and (*b*) bpNO·F_4dIb·bpNO modules extracted from the crystal. Contour maps are shown in the least-squares plane defined by the heavy atoms of the F_4dIb and bpNO molecules. Positive values (step = 0.1 e Å^{-1}) are denoted by solid contours; negative values (step = −0.05 e Å^{-1}) are denoted by dashed contours; wide dashed lines denote zero contours.

agreement being obtained with the DFT calculations. The only discrepancy concerns atoms I and C6, for which the theoretical charges are the opposite of the experimental charges. A possible explanation for this disagreement could be the limited basis set used to describe the I atom in the theoretical calculations, in particular the absence of polarization *f*-type functions. The theoretical net charge on the F_4dIb molecule is $q = -0.04/-0.02$ e from DFT/RHF calculations, in keeping with the sign of the corresponding experimental value.

3.4. Electrostatic potential

Distributions of the electrostatic potential for bpNO·F_4dIb and bpNO·F_4dIb·bpNO modules extracted from the crystal, based on the multipole model (Stewart, 1982), are shown in Fig. 5. The electrostatic interactions are of particular interest for studying both the hydrogen and halogen bonding, and the short intermolecular contacts (see Fig. 1 and Table 3) present in the crystal structure. The electrostatic potential of the bpNO·F_4dIb module (Fig. 5*a*) shows a negative region near the O atoms and a large extension of electronegative potential around F_4dIb, indicating that this molecule is particularly favourable for electrophilic attack. The low electronegative potential in the I···O direction is associated with halogen-bond formation between the bpNO and F_4dIb molecules. The very low electropositive bridge in the I···H region is indicative of a weak interaction; however, a bond path has not been found between the involved atoms. In Fig. 5(*b*), we show the electrostatic potential of a trimer formed by one F_4dIb and two bpNO molecules. Although the magnitude of the electropositive potential is cluster-size dependent, the low bridges of electropositivity connecting the three molecules clearly show the formation of I···H, F···H, O···H and I···O bonds. Lastly, in Fig. 6, we show the electrostatic potential for a cluster formed by three adjacent layers of the same trimer as shown in Fig. 5(*b*). The joint effect of the halogen bonding between the F_4dIb and bpNO molecules, and of the stacking interactions among F_4dIb molecules and among bpNO molecules of different planes, is clearly evidenced.

4. Summary

This work has provided a detailed description of the electron density in the bpNO·F_4dIb complex, which has been compared with the electron density distribution of a previous study of the related bpe·F_4dIb complex (Bianchi *et al.*, 2003). The charge transfer from the bpNO or bpe donor moiety to the F_4dIb acceptor moiety in the two complexes, as determined by both X-ray diffraction at 90 K and quantum mechanical calculations, is practically the same. The negative net charge is distributed among the F, I, O and N atoms, and the positive charge is essentially localized on the C and H atoms of the rings. The chemical reactivity of the bpNO and F_4dIb molecules is satisfactorily explained according to the topology of the Laplacian distribution as well as the electrostatic potential.

The two sets of topological properties determined for the F_4dIb molecule present in both bpNO·F_4dIb and bpe·F_4dIb complexes are reasonably comparable. In particular, the electronic properties of the C—I bond at the BCP appear very similar, pointing in both cases to a description of this bond as being of closed-shell type and characterized by a relatively low and flat electron density distribution. A close similarity was also found between the topological and local energetic properties of the I···O and I···N interactions, confirming the *pure* closed-shell character of the halogen bond and its analogy with hydrogen bonding of medium strength.

The experimental electron density topology suggests an essentially electrostatic nature of the I···O and I···N halogen bonds, as well of the C—H···I, C—H···F and C—H···O hydrogen bonds. The C—H···I interactions are the strongest among the hydrogen bonds present in the crystal, as indicated by the softening-degree (SD) parameter. Other important I···C, N···C and C···C packing interactions present in the crystal structure have been characterized as comparable in strength with the C—H···I hydrogen bonds.

The experimental results are fully confirmed by accurate RHF and DFT theoretical calculations for both intramolecular and intermolecular (if available) BCP properties. In particular, better agreement with the experimental findings is generally shown by the DFT results than by the RHF results. The major discrepancies with experiment concern the topological properties of the polar bonds, whose BCPs are located in regions where the Laplacian changes rapidly, and the net charges of the atoms involved in the C6—I bond.

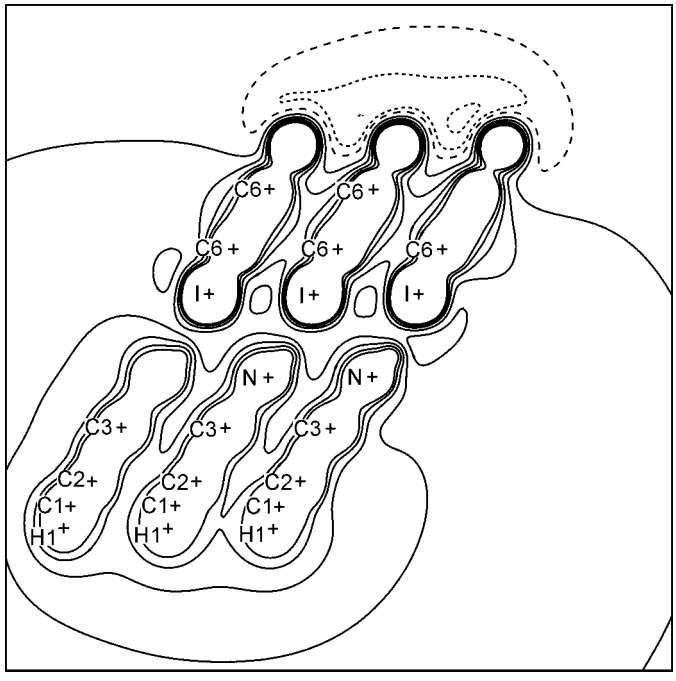

Figure 6
Electrostatic potential for a cluster formed by three adjacent layers of the same trimer, as shown in Fig. 5(*b*). Contour maps are shown in the least-squares plane defined by I, N, C3 and C6 and by the same atoms related by the $(1 + x, y, z)$ symmetry operation. Atom positions within 0.5 Å of the plane are indicated by a + symbol. Contours are as in Fig. 5.

Finally, the hypothesis formulated by Sørensen *et al.* (2003) that an F atom terminally bonded to an aromatic C atom does not possess a significant valence octopole is reinforced by this electron density study.

The authors thank Professor G. Resnati for supplying the crystals.

References

Abramov, Yu. A. (1997). *Acta Cryst.* A**53**, 264–272.

Allen, F. H., Baalham, C. A., Lommerse, J. P. M. & Raithby, P. R. (1998). *Acta Cryst.* B**54**, 320–329.

Allen, F. H., Lommerse, J. P. M., Hoy, V. J., Howard, J. A. K. & Desiraju, G. R. (1997). *Acta Cryst.* B**53**, 1006–1016.

Altomare, A., Cascarano, G., Giacovazzo, C., Guagliardi, A., Burla, M. C., Polidori, G. & Camalli, M. (1994). *J. Appl. Cryst.* **27**, 435.

Andzelm, J., Kłobukowski, M. & Radzio-Andzelm, E. (1984). *J. Comput. Chem.* **5**, 146–161.

Bader, R. F. W. (1994*a*). *AIMPAC*. McMaster University, Hamilton, Ontario, Canada L8S 4M1.

Bader, R. F. W. (1994*b*). *Atoms in Molecules – A Quantum Theory*. Oxford University Press.

Bader, R. F. W. & Beddall, P. M. (1972). *J. Chem. Phys.* **56**, 3320–3329.

Batsanov, A. S., Moore, A. J., Robertson, N., Green, A., Bryce, M. R., Howard, J. A. K. & Underhill, A. E. (1997). *J. Mater. Chem.* **7**, 387–389.

Becke, A. D. (1993). *J. Chem. Phys.* **98**, 5648–5652.

Bianchi, R., Forni, A. & Pilati, T. (2003). *Chem. Eur. J.* **9**, 1631–1638.

Bianchi, R., Gatti, C., Adovasio, V. & Nardelli, M. (1996). *Acta Cryst.* B**52**, 471–478.

Bondi, A. (1964). *J. Phys. Chem.* **68**, 441–451.

Boys, S. F. & Bernardi, F. (1970). *Mol. Phys.* **19**, 553–566.

Bruker (1997). *SMART*, *SAINT* and *SADABS*. Bruker AXS Inc., Madison, Wisconsin, USA.

Burling, F. T. & Goldstein, B. M. (1992). *J. Am. Chem. Soc.* **114**, 2313–2320.

Burnett, M. N. & Johnson, C. K. (1996). *ORTEP*III. Report ORNL-6895. Oak Ridge National Laboratory, Tennessee, USA.

Choudhury, A. R., Urs, U. K., Guru Row, T. N. & Nagarajan, K. (2002). *J. Mol. Struct.* **605**, 71–77.

Desiraju, G. R. (1997). *J. Chem. Soc. Chem. Commun.* pp. 1475–1481.

Desiraju, G. R. & Harlow, R. L. (1989). *J. Am. Chem. Soc.* **111**, 6757–6764.

Desiraju, G. R. & Steiner, T. (1999). *The Weak Hydrogen Bond*. Oxford University Press.

Devic, T., Domercq, B., Auban-Senzier, P., Molinié, P. & Fourmigué, M. (2002). *Eur. J. Inorg. Chem.* pp. 2844–2849.

Espinosa, E., Alkorta, I., Elguero, J. & Molins, E. (2002). *J. Chem. Phys.* **117**, 5529–5542.

Espinosa, E., Molins, E. & Lecomte, C. (1998). *Chem. Phys. Lett.* **285**, 170–173.

Espinosa, E., Souhassou, M., Lachekar, H. & Lecomte, C. (1999). *Acta Cryst.* B**55**, 563–572.

Forni, A., Metrangolo, P., Pilati, T. & Resnati, G. (2004). *Cryst. Growth Des.* **4**, 291–295.

Frisch, M. J. *et al.* (1998). *Gaussian*98. Revision A.9. Gaussian Inc., Pittsburgh, PA, USA.

Garden, S. J., Fontes, S. P., Wardell, J. L., Skakle, J. M. S., Low, J. N. & Glidewell, C. (2002). *Acta Cryst.* B**58**, 701–709.

Gatti, C. (1999). *TOPOND*98 *User's Manual*. CNR–ISTM, Milan, Italy.

Gatti, C. & Bianchi, R. (1996). *VALRAY*95–*TOPOND*. XXVI Congresso Nazionale Associazione Italiana di Cristallografia, Alessandria, Italy, September 1–4, p. 139.

Hamilton, W. C. (1965). *Acta Cryst.* **18**, 502–510.

Hehre, W. J., Ditchfield, R., Stewart, R. F. & Pople, J. A. (1970). *J. Chem. Phys.* **51**, 2769–2773.

Hirshfeld, F. L. (1976). *Acta Cryst.* A**32**, 239–244.

Koritsanszky, T. S. & Coppens, P. (2001). *Chem. Rev.* **101**, 1583–1627.

Lee, C., Yang, W. & Parr, R. G. (1988). *Phys. Rev. B*, **37**, 785–789.

Legon, A. C. (1998). *Chem. Eur. J.* **4**, 1890–1897.

Legon, A. C. (1999*a*). *Angew. Chem.* **111**, 2850–2880.

Legon, A. C. (1999*b*). *Angew. Chem. Int. Ed.* **38**, 2686–2714

Leininger, T., Nicklass, A., Stoll, H., Dolg, M. & Schwerdtfeger, P. (1996). *J. Chem. Phys.* **105**, 1052–1059.

Li, J., Cramer, C. J. & Truhlar, D. G. (1998). *Theor. Chem. Acc.* **99**, 192–196.

Lommerse, J. P. M., Stone, A. J., Taylor, R. & Allen, F. H. (1996). *J. Am. Chem. Soc.* **118**, 3108–3116.

Messina, M. T., Metrangolo, P., Panzeri, W., Pilati, T. & Resnati, G. (2001). *Tetrahedron*, **57**, 8543–8550.

Metrangolo, P. & Resnati, G. (2001). *Chem. Eur. J.* **7**, 2511–2519.

Nardelli, M. (1995). *J. Appl. Cryst.* **28**, 659.

Nishijo, J., Ogura, E., Yamaura, J., Miyazaki, A., Enoki, T., Takano, T., Kuwatani, Y. & Iyoda, M. (2000). *Solid State Commun.* **116**, 661–664.

Sørensen, H. O., Stewart, R. F., McIntyre, G. J. & Larsen, S. (2003). *Acta Cryst.* B**59**, 540–550.

Stewart, R. F. (1976). *Acta Cryst.* A**32**, 565–574.

Stewart, R. F. (1982). *God. Jugosl. Cent. Kristalogr.* **17**, 1–24.

Stewart, R. F. & Spackman, M. A. (1983). *VALRAY User's Manual*. Department of Chemistry, Carnegie–Mellon University, Pittsburgh, USA.

Stewart, R. F., Spackman, M. A. & Flensburg, C. (2000). *VALRAY User's Manual*. Version 2.1. Department of Chemistry, Carnegie–Mellon University, Pittsburgh, PA, USA, and University of Copenhagen, Denmark.

Thalladi, V. R., Weiss, H.-C., Bläser, D., Boese, R., Nangia, A. & Desiraju, G. R. (1998). *J. Am. Chem. Soc.* **120**, 8702–8710.